Published in final edited form as:
J Immunol. 2012 November 1; 189(9): 4602–4611. doi:10.4049/jimmunol.1200486.

Cross-Immunoreactivity between Bacterial Aquaporin-Z and Human Aquaporin-4: Potential Relevance to Neuromyelitis Optica

Zhihua Ren[*,1], **Yan Wang**[*,1], **Tao Duan**[*,1], **Jilpa Patel**[*,1], **Thomas Liggett**[*], **Eileah Loda**[*], **Sarang Brahma**[*], **Rajendra Goswami**[*], **Carrie Grouse**[*], **Richard Byrne**[†], **Dusan Stefoski**[*], **Adil Javed**[‡], **Stephen D. Miller**[§], and **Roumen Balabanov**[*]

[*]Department of Neurological Sciences, Multiple Sclerosis Center, Rush University Medical Center, Chicago, IL 60612

[†]Department of Neurosurgery, Rush University Medical Center, Chicago, IL 60612

[‡]Department of Neurology, University of Chicago, Chicago, IL 60637

[§]Department of Microbiology-Immunology, Northwestern University Medical School, Chicago, IL 60611

Abstract

Neuromyelitis optica (NMO) is a chronic inflammatory disease of the CNS that is mediated, in part, by a self-reactive Ab against the astrocyte aquaporin-4 protein. In the current study, we examined the possibility and the biological significance of cross-immunoreactivity between bacterial aquaporin-Z and human aquaporin-4 proteins. Sequence-alignment analysis of these proteins revealed several regions of significant structural homology. Some of the homologous regions were also found to overlap with important immune and disease-relevant epitopes. Cross-immunoreactivity between aquaporin-Z and aquaporin-4 was investigated and ascertained in multiple immune-based assays using sera from patients with neuromyelitis optica, immune mouse serum, and Abs raised against aquaporin-Z. The biological significance of this phenomenon was established in series of experiments demonstrating that induction of an immune response against aquaporin-Z or its homologous regions can also trigger an autoimmune reaction against aquaporin-4 and inflammation of the CNS. Our study indicates that the autoimmune response against aquaporin-4 in neuromyelitis optica may be triggered by infection-induced cross-immunoreactivity and presents a new perspective on the pathogenesis of this disease.

Neuromyelitis optica (NMO) is a chronic inflammatory disease of the CNS (1). NMO characteristically involves the optic nerves and the spinal cord of patients, causing visual loss and myelopathy. Pathological abnormalities of the disease include inflammatory cell infiltration, Ig and complement deposition, tissue necrosis, and demyelination that are typically localized within the perivascular spaces (2). Although the etiology of NMO is unknown, it is believed to be an autoimmune disorder (2, 3). NMO has been associated with other autoimmune disorders, suggesting the existence of a genetic predisposition (4, 5). A

Address correspondence and reprint requests to Dr. Roumen Balabanov, Multiple Sclerosis Center, Department of Neurological Sciences, Rush University Medical Center, 1725 W. Harrison Street, Suite 309, Chicago, IL 60612. Roumen_Balabanov@rush.edu.

[1]Z.R., Y.W., T.D., and J.P. contributed equally to this work and share first authorship.

The online version of this article contains supplemental material.

Disclosures The authors have no financial conflicts of interest.

potential role for a microbial trigger has also been hypothesized based on circumstantial associations of the disease with certain infections (6). There is no cure for NMO; all of the available immunotherapies have only partial efficacy and uncertain long-term benefit.

Aquaporins (Aqp) represent a family of transmembrane proteins that regulate water flow in cells (7). They are expressed by various mammalian cell types and bacteria, and they display similar three-dimensional loop/helix structure across the plasma membrane (8). Mutations in certain aquaporin genes have been associated with human hereditary diseases (9). Aqp4 has been proposed as the primary autoimmune target in NMO based on the presence of a self-reactive anti-Aqp4 Ab in patients' sera (10–13). Aqp4 is a 35-kDa protein that is expressed by the CNS astrocytes and their cell processes surrounding the small blood vessels (14–19). Aqp4 is the main water channel of the CNS, and its dysfunction compromises the local homeostasis (20–23). AqpZ is a common bacterial aquaporin that was originally described in *Escherichia coli* (24, 25). It is a 27-kDa protein that also functions as a water channel regulating bacterial cell volume and osmotic stress (26).

Cross-immunoreactivity is a phenomenon of structural homology between foreign and self molecules that can trigger a non-discriminatory immune response (27). This phenomenon is immunologically possible because of the degeneracy of the immune receptors and the promiscuous mechanisms of Ag recognition (28). Infection-induced cross-immunoreactivity has been implicated in the pathogenesis of a number of autoimmune disorders of the nervous system (29–31). Theoretically, it provides a mechanistic model of conversion of a normal antimicrobial immune response into an abnormal autoimmune response and disease. Given the autoimmune nature of NMO, one can hypothesize that the autoimmune response against Aqp4 may arise through a mechanism of cross-immunoreactivity with a microbial molecule.

In the current study, we provide direct evidence for the existence of structural homology and cross-immunoreactivity between bacterial AqpZ and human Aqp4 proteins. Our study indicates that infection-induced cross-immunoreactivity is likely to play a role in the induction of the anti-Aqp4 response in NMO.

Materials and Methods

Recombinant Aqp4 and AqpZ proteins

cDNA of human Aqp4 (accession no. NM_ 001650.4) and *E. coli* AqpZ (gene identifier 945497; protein identifier NP 415396.1) (http://www.ncbi.nlm.nih.gov) were commercially synthesized (Sigma Gene Synthesis, St. Louis, MO). Aqp4 cDNA was subcloned into a bacterial expression vector pEcoli-C term 6×HN (Clontech, Mountain View, CA) containing a His-tag sequence. BL21/DE3 bacteria were transfected with the recombinant vector, and the expression of Aqp4 protein was induced by administration of 3 mM isopropyl β-D thiogalactopyranoside (IPTG) overnight at 37°C. Aqp4 protein was purified using a HisTALON Gravity Columns Purification Kit (Clontech). Recombinant AqpZ protein was generated using pMAL protein fusion and a purification system (New England Biolabs, Ipswich, MA). AqpZ cDNA was subcloned into a pMAL-c4X bacterial expression vector containing the MBP gene. AqpZ-MBP fusion protein was also expressed in BL21/DE3 bacteria using IPTG and isolated using maltose-dependent elution. AqpZ was cleaved from MBP with Factor Xa protease and then affinity purified. Aqp4 and AqpZ were isolated in the absence of reducing agents and kept in PBS (pH 7.4) to prevent denaturation. The purity of recombinant Aqp4 and AqpZ proteins was determined by 8–16% gradient SDS-PAGE, followed by endotoxin testing, mass spectroscopy, and Western blot.

Human and mouse sera and anti-AqpZ$_{180–207}$ and anti-AqpZ$_{174–190}$ IgGs

Human serum samples were obtained from patients with NMO (n = 20 samples) and normal individuals (n = 9 samples) using a standard laboratory procedure. Diagnosis of NMO was established based on the revised diagnostic criteria of the disease (32). All patients tested positive for NMO (anti-Aqp4) Ab in a diagnostic laboratory (Mayo Medical Laboratories, Rochester, MN). Immune mouse serum against AqpZ was produced by repeated (three times, 10 d apart) immunizations of 6–8-wk-old female SJL/J mice (The Jackson Laboratory, Bar Harbor, ME). Mice received 300 μg AqpZ protein, emulsified in CFA containing 600 μg *Mycobacterium tuberculosis* (Difco, Detroit, MI), intradermally, as we described previously (33). Control serum was obtained from mice injected with CFA only.

Anti-AqpZ$_{180–207}$ and anti-AqpZ$_{174–190}$ IgGs were produced at the Proteomic Facility of University of Illinois at Chicago by immunizing New Zealand white rabbits with AqpZ$_{180–207}$ (VTNTSVNPARSTAVAIFQGG-WALEQLWF) or AqpZ$_{174–190}$ (HLISIPVTNTSVNPARS) peptides conjugated to keyhole limpet hemocyanin. The IgG fraction was purified using high-affinity chromatography and reconstituted in PBS at a concentration of 2 mg/ml.

ELISA and a latex agglutination assay

Indirect ELISA with Aqp4 and AqpZ proteins was performed using an eBioscience kit (eBioscience, San Diego, CA), as we detailed before (33). ELISA plates were coated separately with Aqp4 or AqpZ proteins (0–20 μg/well) or with Aqp4$_{207–232}$ (YTGASMNPARSFGPAVIMG NWENHWI), Aqp4$_{201–217}$ (HLFAINYTGASMNPARS), AqpZ$_{180–207}$, AqpZ$_{174–190}$, or AqpZ$_{67–80}$ (TIGLWAGGRFPAKE) peptides (University of Illinois Proteomic Facility) (2 μg/well). Human or mouse sera (1:100–1:1600 dilution in 1% BSA/PBS) or anti-AqpZ$_{180–207}$ or anti-AqpZ$_{174–190}$ IgGs (1:500 dilution in 1% BSA/PBS) were added to the wells for 1 h at 37°C. Blank or trypsin inhibitor-coated wells were used as negative controls. ELISA reaction was measured in OD units at a wavelength of 450 nm.

A latex agglutination assay was performed according to a previously published protocol, with modifications (34). FITC or cyanin (Cy)3 latex beads (0.5 μm, 10 μl) (Sigma-Aldrich, St. Louis, MO) were coated with Aqp proteins (2 mg protein/ml of beads) and then mixed with either human serum (1:50 dilution) or an anti-human Aqp4 Ab (1:100 dilution; cat. no. SC-20812, Santa Cruz Biotechnology, Santa Cruz, CA) in 50 μl 25 mM MES buffer. The agglutination reaction was allowed to proceed for 2 h at room temperature and was monitored under a fluorescent microscope (Axioplan digital microscope, Zeiss, Thornwood, NY).

Western blot and immunoprecipitation

Western blot and immunoprecipitation (IP) were performed, as we described previously (33, 35). Protein samples (50–100 μg) were resolved on 8–16% SDS-PAGE and immunoblotted with an anti-Aqp4 Ab (1:100 dilution; Santa Cruz Biotechnology) or with sera (1:100 dilution), followed by species-matched infrared-labeled secondary Abs (1:10,000 dilution; LI-COR Biosciences, Lincoln, NE). IP was performed by coin-cubating cell lysates (100 μg protein) and serum samples (5 μl, 1:10 dilution) in 600 μl volume overnight at 4°C, followed by Sepharose beads precipitation (Santa Cruz Biotechnology) and Western blotting.

Mouse immunizations

Six- to eight-week-old female SJL/J mice were immunized with 300 μg AqpZ protein or a mixture containing equal ratios of homologous AqpZ peptides (AqpZ$_{55–67}$ [GHISGGHFNPAVT], AqpZ$_{82–101}$ [VGYVIAQVVGGIVAAALLYL], AqpZ$_{174–190}$, and

$AqpZ_{203–220}$ [EQLWFFWVVPIVPGIIGG]) or homologous Aqp4 peptides ($Aqp4_{89–101}$ [GHISGGHINPAVT], $Aqp4_{116–135}$ [VFYIAAQCLGAIIGAGILYL], $AqpZ_{201–217}$, and $Aqp4_{228–245}$ [ENHWIYWVGPIIGAVLAG]) (University of Illinois Proteomic Facility) and emulsified in CFA, as we reported previously (33, 36). Control mice were injected with CFA only. All of the mice also received 100 ng pertussis toxin (List Biological Laboratories, Campbell, CA) i.p. 24 h postimmunization (PI). Experimental animals were examined daily for signs of clinical disease. Sensory testing was performed by applying painful stimuli (pin prick) to animals' tails and limbs, and their withdrawal responses were recorded. A semiquantitative scale was used to describe the severity of sensory loss: 0, no sensory loss (quick withdrawal) to pain; 1, diminished response (weak withdrawal not due to muscle weakness) to pain; 2, lack (absence of withdrawal not due to muscle weakness) of pain reaction, 3, nondistressful mutilated tail.

Intracerebral injections

Intracerebral injection of an anti-$AqpZ_{174–190}$ IgG was performed stereo-tactically into the left brain hemisphere of the mice using a 33-gauge needle. Each injection delivered 8 μg anti-$AqpZ_{174–190}$ IgG and 2 μl 5% Low-Tox H rabbit complement (Cedarlane Labs, Burlington, NC). Complement alone or together with an isotype IgG were also injected as controls. Experimental animals were examined, and their spontaneous motor activity was measured by an automated activity monitoring system (Digiscan; Omnitech Electronics, Columbus, OH). Movement time for each animal was recorded separately in 10 sessions (5 min/session) on day 8 posttreatment. Cumulative time in minutes was calculated, and data were analyzed using systems' software.

Histochemistry and immunohistochemistry

Tissue samples were prepared as frozen blocks and stained with H&E using our standard laboratory protocol (36). Indirect immunostaining was performed as we described previously using mouse (1:500 dilution) or human sera (1:100 dilution), anti-$AqpZ_{174–190}$ IgG (1:500 dilution), anti-glial fibrillary acidic protein (GFAP; 1:1,000 dilution; Dako, Glostrup, Denmark), anti-CD3 (1:200 dilution; Santa Cruz Biotechnology), LN3 (1:500 dilution, MP Biomedical, Santa Ana, CA), anti-C5b-9 (1:200 dilution; Abcam, Cambridge, MA), anti-Aqp4 (1:100 dilution; Santa Cruz Biotechnology), anti-IL-17a (1:100 dilution; BD Bioscience, San Jose, CA), and anti-BrdU (1:100 dilution; Abcam) Abs, as well as isotype control IgG (in corresponding dilutions; Sigma-Aldrich), followed by species-matched FITC-conjugated, Cy3-conjugated, or biotinylated secondary Abs (Vector Laboratories, Burlingame, CA) (35, 36). Diaminobenzidine (DAB) and DAB/$NiSO_4$ (Sigma-Aldrich) were used as reaction substrates for the biotinylated Abs. Cell nuclei were stained using DAPI (Vector Laboratories). Quantitative analysis of inflammatory foci (inflammatory focus was defined as presence of >20 inflammatory cells in a cluster or around a blood vessel) within a given area (digitally selected in mm^2) was performed, as we described previously in detail (33, 36). Data were collected and processed using Axiovision software of the Axioplan digital microscope (Zeiss).

Immunostaining of HEK cells was performed as described above. In these experiments, HEK 293 cells (1×10^5/well) were transfected with pcDNA3.1 vector (1 μg plasmid DNA) carrying either Aqp4 or AqpZ cDNA, as we described previously (35). NMO sera (200 μl) were preabsorbed with AqpZ (700 μg) overnight at 4°C.

Cell-viability assay

Human astrocyte cultures were generated from epilepsy brain tissue using previously described protocols (35, 37). Astrocytes were cultured in 96-well plates (1×10^5 cells/well) and then treated with control human or NMO sera (1:3 dilution), anti-$AqpZ_{180–207}$, anti-

$AqpZ_{175–191}$, or control isotype IgGs (50 μg/ml) in the presence or absence of rabbit complement (1:50 dilution of the commercial 5% stock) (Cedarlane Labs) for 2 h at 37°C. Cell viability was assessed using an MTT colorimetric assay, as we described previously (33, 35). The results are presented as mean (± SD) percentage viability, for which untreated control cells were considered to be 100%.

Lymphocyte-proliferation assay and flow cytometry

A lymphocyte-proliferation assay was performed at day 8 PI using purified spleen T cells obtained from mice immunized with either AqpZ proteins or homologous AqpZ peptides or from CFA-injected mice, as we detailed previously (33, 36, 38). T cells were isolated by compressing the spleens against a metallic mesh and filtration though a 30-μm filter. Subsequently, they were purified by selective nonadherence to nylon wool fiber columns (Polysciences, Warrington, PA), according to the manufacturer's protocol. AqpZ, Aqp4, and $OVA_{323–339}$ (Genemed Synthesis, San Francisco, CA) peptides were added to the cultures (0–50 μg/ml for 72 h), and cell proliferation was measured by a BrdU-incorporation assay (Calbiochem, La Jolla, CA). Con A (5 μg/ml/72h) (Sigma-Aldrich) was added to certain cultures as well. Multicolor flow cytometry was performed to assess for lymphocyte population changes, as we described previously (36, 38). Immunostaining was performed using anti-CD4/FITC (1:100 dilution), anti-IFN-γ/PerCP-Cy5.5 (1:100 dilution), anti-IL-17a/allophycocyanin-Cy7 (1:100 dilution), and anti-IL-4/PE (1:100 dilution) Abs (BD Bioscience).

Institutional approval for human and animal experimentation

All human and animal studies were approved by the institutional review board(s) of Rush University Medical Center.

Statistical analysis

Comparison of variables was performed using one-way ANOVA in the SPSS program (SPSS, Chicago, IL). The results are presented as mean ± SD of the measured variable. A statistically significant difference was defined as a p value < 0.05, with $n \geq 3$ experiments.

Results

Structural homology between Aqp4 and AqpZ proteins

Amino acid sequences of human Aqp4 and *E. coli* AqpZ proteins were examined for structural homology using the ExPASy Proteomics Server software (Swiss Institute of Bioinformatics) (Fig. 1A). Aqp4 is a single-chain protein with two isoforms: M1 (full length) and M23 (shorter splice variant) composed of 323 and 301 aa, respectively. AqpZ is a single-chain protein composed of 231 aa. The primary amino acid sequence of both proteins predicted the formation of six transmembrane α helices and five interhelical loops (three extracellular and two intracellular loops) (Supplemental Fig. 1).

Sequence-alignment analysis of Aqp4 and AqpZ proteins revealed that they shared ~20% homology, with various levels of clustering along their length. The same homologous amino acids were present in M1 and M23 isoforms of Aqp4. Four regions with significant structural homology were identified: region 1 (90% homology), comprising 13 residues corresponding to $Aqp4_{89–101}$ and to $AqpZ_{55–67}$; region 2 (50% homology), comprising 20 residues corresponding to $Aqp4_{116–135}$ and to $AqpZ_{82–101}$; region 3 (60% homology), comprising 17 residues corresponding to $Aqp4_{201–217}$ and to $AqpZ_{174–190}$; and region 4 (45% homology), comprising 18 residues corresponding to $Aqp4_{228–245}$ and to $AqpZ_{203–220}$.

Identified regions of homology were found to overlap with a number of immune epitopes relevant to NMO. Specifically, the third extracellular loop of Aqp4 (residues 207–232), believed to be a binding site of anti-Aqp4 Ab in NMO and a potential T cell epitope in experimental animals, shared ~45% (12 of 25 aa) homology with the corresponding domain in AqpZ (residues 180–207) (18, 19, 39). This extracellular loop contains portions of homologous regions 3 and 4, as well as three individual homologous residues in between. Significant overlap between other reported Aqp4 T cell epitopes and the regions of homology were recognized as well (40, 41).

Immune (AqpZ) mouse serum cross-reacted with Aqp4 protein

The presence of structural homology between Aqp4 and AqpZ prompted us to examine whether immune mouse serum raised against recombinant AqpZ protein would cross-react with Aqp4. For this purpose, we generated recombinant Aqp4 (M1) and AqpZ proteins. The recombinant proteins had the predicted molecular mass of 35 kDa for Aqp4 and 27 kDa for AqpZ (Fig. 1B, 1C). In a Western blot assay, Aqp4 was recognized by a commercial anti-Aqp4 Ab and the AqpZ by an immune mouse serum against this protein (Fig. 1D, 1E).

Immune (AqpZ) mouse serum was generated as detailed above and examined for reactivity against AqpZ and cross-reactivity against Aqp4. Testing was performed against control sera using an indirect ELISA, IP, and immunohistochemistry (Fig. 2, Supplemental Fig. 2). ELISA demonstrated that immune (AqpZ) mouse serum produced a strong dose-dependent signal with both AqpZ and Aqp4, which was significantly higher compared with the control mouse serum at multiple dilutions. The maximum differences were observed with 1:100 serum dilution and 10 μg of capturing protein (AqpZ, 2.1 ± 0.1 versus 0.23 ± 0.1 OD units for the immune and control sera, respectively; Aqp4, 0.51 ± 0.02 versus 0.17 ± 0.01 OD units for the immune and control sera, respectively; $p < 0.05$ for both comparisons, $n = 3$ measurements) (Fig. 2A, Supplemental Fig. 2). Immune serum and control sera reacted minimally and at levels comparable to trypsin inhibitor (irrelevant protein control) under the same conditions: 0.19 ± 0.2 and 0.16 ± 0.17, respectively ($p > 0.05$, $n = 3$ measurements). In the IP experiments, cell lysates of BL21/DE3 bacteria over-expressing Aqp4 were incubated with immune (AqpZ) mouse, NMO, or control sera, and the presence of Aqp4 in the immunoprecipitates was examined using Western blot with the commercial anti-Aqp4 Ab. Bands with the expected molecular mass of 35 kDa for Aqp4 were detected in both reactions and were produced with the immune (AqpZ) mouse and NMO sera but not with the control sera (Fig. 2B, 2C). Reactions with trypsin inhibitor were also negative. Immunostaining of human astrocyte cell cultures and brain tissue with immune (AqpZ) mouse serum generated strong immunopositive signals that colocalized exclusively with the astrocytes (Fig. 2D–K, Supplemental Fig. 3). In these experiments, anti-GFAP Ab (an astrocyte cell marker) and commercial anti-Aqp4 Ab were used to control for cellular localization of immunopositivity. Concurrently used control serum and isotype IgG did not generate any immunopositive signals.

NMO sera cross-reacted with AqpZ proteins

Testing for NMO serum cross-reactivity with AqpZ was similarly performed using an indirect ELISA, Western blot, immunostaining, and latex agglutination (Fig. 3, Supplemental Fig. 4). ELISA demonstrated significantly higher reactivity of NMO sera ($n = 20$) with AqpZ compared with control serum ($n = 9$): 1.1 ± 0.3 versus 0.52 ± 0.1 OD units, respectively, at 1:100 serum dilution and 10 μg of capturing protein ($p < 0.05$) (Fig. 3A). Western blots carried out using AqpZ protein, NMO sera, and the above-mentioned commercial anti-Aqp4 Ab (1:100 dilution for both) produced bands with the expected molecular mass of 27 kDa for AqpZ (Fig. 3B, 3C). No bands were observed with normal human sera and isotype IgG, which were used as negative controls in the experiments.

Immunostaining was performed using Aqp4- and AqpZ-overexpressing HEK cells and NMO sera that was preabsorbed with AqpZ (Fig. 3D–I). Sham-transfected HEK cells and untreated NMO sera were used as controls. Strong immunopositivity was observed with the untreated NMO sera (1:100 dilution) and the Aqp4- and AqpZ-overexpressing HEK cells but not with the control HEK cells. In contrast, little immunopositivity was detected in the same cell cultures when the AqpZ-preabsorbed NMO sera was used. The agglutination assay was performed using a mixture of Aqp4-coated (Cy3-labeled) and AqpZ-coated (FITC-labeled) latex beads and the NMO or control sera, or the commercial anti-Aqp4 Ab. The assay resulted in the appearance of mixed aggregates containing both Aqp4- and AqpZ-coated beads with the NMO sera and the commercial anti-Aqp4 Ab but not with the control human sera (Supplemental Fig. 4).

Cytotoxicity of anti-AqpZ IgGs

It was previously demonstrated that NMO sera exert a cytotoxic effect on astrocytes in vitro (17). We addressed the question whether Abs generated against the homologous extracellular regions of AqpZ would demonstrate similar properties. We generated rabbit IgGs against synthetic peptides containing the $AqpZ_{180–207}$ (third extracellular loop) and $AqpZ_{174–190}$ (region 3 of homology and a part of the third extracellular loop) residues. Region selection was based on our sequence-alignment analysis. As designed, the newly generated anti-$AqpZ_{180–207}$ IgG (1:5,000 dilution) reacted with $AqpZ_{180–207}$ and cross-reacted with the homologous $Aqp4_{207–232}$ peptides (2 mg/well): 0.29 ± 0.08 and 0.24 ± 0.07 OD units, respectively ($n = 3$ measurements) (Fig. 4A). Similarly, anti-$AqpZ_{174–190}$ IgG demonstrated reactivity with $AqpZ_{174–190}$ and cross-reactivity with the homologous $Aqp4_{201–217}$ peptides: 0.22 ± 0.03 and 0.2 ± 0.02 OD units, respectively ($n = 3$ measurements). These reactivities were significantly higher compared with those produced under the same conditions with the nonhomologous $AqpZ_{67–80}$ peptide: 0.04 ± 0.002 OD units with anti-$AqpZ_{180–207}$ IgG and 0.05 ± 0.003 OD units with anti-$AqpZ_{174–190}$ IgG ($n = 3$ measurements; $p < 0.05$ for each comparison).

Ab-mediated cytotoxicity was examined in vitro using both anti-AqpZ IgGs (Fig. 4B). In these experiments, cultured human astrocytes (1×10^5 cells/well) were treated separately with anti-$AqpZ_{180–207}$ IgG, anti-$AqpZ_{174–190}$ IgG, and control isotype IgG (50 μg/ml for all) in the presence or absence of rabbit complement (1:50 dilution), and their cell viability was tested after 2 h of treatment. Control human and NMO sera (1:3 dilution) were used as biological controls. The cytotoxic assays demonstrated that anti-AqpZ IgGs have the capacity to bind to astrocytes, to activate complement, and to cause significant cell death. Cell viabilities assessed by an MTT assay in the anti-$AqpZ_{180–207}$ IgG-, the anti-$AqpZ_{174–190}$ IgG-, and the NMO serum-treated cultures were significantly reduced to 41.4 ± 1.35, 25.8 ± 1.45, and 16.9 ± 3.2%, respectively, in comparison with the controls of each test ($p < 0.05$, $n = 3$ measurements). Formation of the C5b-9 membrane attack complex (a marker of complement activation) was observed in the astrocyte cultures within 20 min of the cytotoxic assay (Fig. 4C–F).

Intracranial injection of anti-$AqpZ_{174–190}$ IgG caused CNS inflammation

The capacity of anti-$AqpZ_{174–190}$ IgG to induce CNS inflammation was also studied in a model of intracerebral injection (42). A mixture of the Ab, either anti-$AqpZ_{174–190}$ or control IgG (8 μg), and complement (2 μl) was injected stereotactically in the brains (left hemisphere) of SJL/J mice. Contralateral brain hemispheres of the experimental animals were used as tissue controls. All mice injected with the anti-$AqpZ_{174–190}$ IgG exhibited sick behavior several days after the injection, including behavioral withdrawal and limited spontaneous movements. In contrast, isotype IgG-injected mice appeared to be clinically normal. Quantitatively, movement time measured for 50 min of anti-$AqpZ_{174–190}$ IgG -

injected mice was significantly diminished compared with isotype IgG-injected control mice: 13.2 ± 2.1 versus 37.8 ± 4 min, respectively, at day 8 posttreatment (n = 10 animals/group, $p < 0.05$). Histological analysis of anti-$AqpZ_{174–190}$ IgG-injected mice also done at day 8 posttreatment demonstrated accumulation of inflammatory cells and formation of C5b-9 membrane attack complex (n = 3 animals/group) (Fig. 5). Isotype IgG-injected mice demonstrated little inflammation or complement activation. No histological abnormalities were observed in the untreated mice or in the mice treated with complement only (Fig. 5).

Immunization of SJL/J mice with AqpZ protein/peptides caused CNS inflammation

Proliferative and encephalitogenic T cell responses against Aqp4 epitopes have been described in experimental animals (39, 40). We investigated the encephalitogenic properties of AqpZ protein and its homologous peptides in an active-immunization model. Six- to eight-week-old female SJL/J mice were immunized either with AqpZ protein (nine mice) or with a mixture of its homologous peptides ($AqpZ_{55–67}$, $AqpZ_{82–101}$, $AqpZ_{174–190}$, $AqpZ_{203–220}$) in equal ratios (six mice). Additional mice were similarly immunized with a mixture of the corresponding Aqp4 homologous peptides ($Aqp4_{89–101}$, $Aqp4_{116–135}$, $AqpZ_{201–217}$, $Aqp4_{228–245}$) or injected with CFA only (six mice/each group). Mice immunized with either AqpZ protein or its homologous peptides developed a disease ~60 d PI thatlastedfor >30 d. The clinical signs of the disease included loss of sensation to pain in the hind limbs and tail. Sensory loss was observed in seven of nine of the AqpZ protein-immunized mice (maximum score = 2.7 ± 1), five of six of the AqpZ peptide-immunized mice (maximum score = 2.3 ± 3), and all six of the Aqp4 peptide-immunized mice (maximum score = 2.5 ± 3). Histological examination of randomly selected mice (n = 3 animals/group) at day 60 PI demonstrated that sensory loss in the animals was associated with spinal cord inflammation consisting of mononuclear infiltration of the meninges, subependymal areas, and perivascular spaces. These were most commonly present in the spinal cords' posterior columns (Fig. 6A–D). Numerically, the inflammatory foci among the immunized mice were comparable: 7.2 ± 2.6/mm^2 in the AqpZ protein-immunized mice, 9.3 ± 1.5/mm^2 in the Aqp4 peptide-immunized mice, and 8.1 ± 3.4/mm^2 in the Aqp4 peptide-immunized mice. The inflammatory infiltrates consisted of $CD3^+$ (a lymphocyte marker) and $LN3^+$ (a monocyte cell marker) cells, and they were localized within the $Aqp4^+$ areas of the spinal cords (Fig. 6E–T). Overall, the clinical findings and the CNS pathology induced by AqpZ protein/peptides were comparable to those induced by the homologous Aqp4 peptides. No significant clinical or histological abnormalities were observed in the CFA-injected mice.

T cell cross-reactivity between AqpZ and Aqp4 peptides

Spleen T cells were isolated from SJL mice that had been immunized separately with the homologous $AqpZ_{55–67}$, $AqpZ_{82–101}$, $AqpZ_{174–190}$, and $AqpZ_{203–220}$ peptides or with AqpZ protein or were isolated from CFA-injected mice at day 8 PI (n = 3 animals/group). Their responses to the priming AqpZ peptide, a non-priming but homologous (Aqp4) peptide, and a nonpriming and nonhomologous $OVA_{323–339}$ peptide (0–50 μg/ml/72 h) were tested in a lymphocyte-proliferation assay (Fig. 7A–F). The experiments demonstrated that T cells of the $AqpZ_{82–101}^-$, $AqpZ_{174–190}^-$, and $AqpZ_{203–220}^-$immunized mice had the capacity to proliferate upon stimulation with the priming peptides, as well as with the corresponding homologous $Aqp4_{116–135}$, $Aqp4_{201–217}$, and $Aqp4_{228–245}$ peptides, respectively (Fig. 7A–C). Little cell proliferation was observed in the assays using T cells from the $AqpZ_{55–67}^-$immunized mice (data not shown). Maximum proliferation was detected with T cells obtained from $AqpZ_{174–190}^-$immunized mice that were stimulated with 20 mg/ml of $AqpZ_{174–190}$ and $Aqp4_{201–217}$: 1.03 ± 0.08 and 0.61 ± 0.06 OD units, respectively (Fig. 7B). These proliferative responses were significantly higher compared with the one elicited from the same cultures with $OVA_{323–339}$ (0.19 ± 0.02 OD units; $p < 0.05$ for both comparisons).

In addition, strong proliferative responses to the same AqpZ and Aqp4 peptides were observed with T cells from mice immunized with the full-length AqpZ protein (Fig. 7D–F). For instance, T cell proliferation in response to $AqpZ_{174–190}$ and $Aqp4_{201–217}$ was significantly higher compared with $OVA_{323–339}$: 0.71 ± 0.03, 0.6 ± 0.1, and 0.13 ± 0.01 OD units, respectively, with 20 μg/ml ($p < 0.05$ for both comparisons) (Fig. 7E). Lymphocyte proliferative responses in the absence of Ag priming (CFA only) were low and close to the background. Independently, the presence of T cell proliferation in these assays was ascertained using dual immunostaining with anti-$CD3^+$ and anti-BrdU Abs (Fig. 7G–O).

We also looked for changes in the IFN-γ^+/$CD4^+$ (Th1), IL-4^+/$CD4^+$ (Th2), and IL-$17a^+$/$CD4^+$ (Th17) cell populations. Using flow cytometry, we found that stimulation of the $AqpZ_{174–190}$−and $AqpZ_{203–220}$−primed T cells with the same AqpZ and corresponding homologous Aqp4 peptides (20 μg/ml/72 h) was associated with a relative increase in the IL-$17a^+$/CD^+ cells (Fig. 8A, 8B). The other tested CD4 populations remained unchanged (data not shown). The percentage of IL-$17a^+$/$CD4^+$ cells increased significantly with $AqpZ_{174–190}$ and $Aqp4_{201–217}$ stimulation compared with medium only: 2.2 ± 0.18 and 1.34 ± 0.09% versus 0.6 ± 0.09%, respectively ($p < 0.05$ for both comparisons). They were similarly increased with $AqpZ_{203–220}$ and $Aqp4_{228–245}$ stimulation compared with medium only: 1.53 ± 0.12 and 2.5 ± 0.13% versus 0.76 ± 0.09%, respectively ($p < 0.05$ for both comparisons). No significant change in this cell population was observed in the absence of Ag priming (CFA only). Con A stimulation (5 μg/ml) of the same cultures resulted in a significant increase in IL-$17a^+$/$CD4^+$ cells, irrespective of priming (range 10–16%). In corroboration, we detected IL-$17a^+$ cells within the inflammatory infiltrates of all immunized mice (Fig. 8C–H).

Discussion

NMO is an autoimmune disorder of the CNS that is mediated, in part, by a self-reactive Ab against astrocyte Aqp4 protein. The goal of this study was to examine whether an autoimmune response against Aqp4 may arise through a mechanism of infection-induced cross-immunoreactivity. We analyzed the amino acid sequence of bacterial (*E. coli*) AqpZ and human Aqp4 proteins and identified four homologous regions with corresponding transmembrane localization. The most important finding of this analysis was that some of the homologous residues overlapped with an Aqp4 domain (the third extracellular loop) thought to be an immune target in NMO and of encephalitogenic significance (18, 19, 39–41). Next, we generated recombinant AqpZ and Aqp4 proteins, as well as homologous synthetic peptides, and tested them for cross-immunoreactivity using sera from patients with NMO and immune mouse sera raised against a recombinant AqpZ protein. Cross-immunoreactivity between AqpZ and Aqp4 was observed in multiple independent assays, including ELISA, Western blot, IP, immunohistochemistry, and latex agglutination. We also demonstrated that Abs raised against homologous regions of AqpZ have the capacity to cross-react with their Aqp4 counterparts, cause astrocyte cell death, and trigger CNS inflammation. Finally, we described induction of CNS inflammation in mice upon active immunization with AqpZ protein or homologous AqpZ and Aqp4 peptides, which was associated with T cell cross-reactivity between them. Based on these results, we concluded that bacterial AqpZ and human Aqp4 proteins share significant structural homology and cross-react in immune-based assays and experimental systems. Thus, our study provides direct evidence that infection-induced cross-reactivity may be involved in the induction of the autoimmune response against Aqp4 in NMO. The findings of our study are novel and provide a new perspective on the pathogenesis of NMO.

Our study indicates involvement of a bacterial pathogen in NMO. Microbial trigger has also been considered in several reports, based upon circumstantial associations of certain

infections with the disease onset (e.g., *Mycobacterium tuberculosis* and *Helicobacter pylori*) (6, 43–45). In addition, Th17 cells mediating host defense against extracellular bacteria are involved in NMO and can be activated by a synthetic bacterial epitope in vitro (the latter was reported as a rapid communication during the revisions of our manuscript) (46–49). Hypothetically, a bacterial infection (symptomatic or occult) and the ensuing inflammatory reaction may compromise the process of self and nonself discrimination of AqpZ and induce an autoimmune response against Aqp4. For instance, urinary tract infections (including *E. coli*) occurring secondary to myelopathy can trigger a disease relapse or worsening. Other factors in addition to exposure to bacterial pathogens are likely to play a role in the disease pathogenesis as well. NMO has been associated with specific HLA (the Ag-presenting molecule in humans) types, which may preferentially bias the anti-bacterial immune response against the homologous regions of AqpZ, a mechanism that can explain why NMO is a rare disease despite the abundance of AqpZ in the environment (39, 50). Species variability and dynamic changes in AqpZ amino acid sequence may account for this phenomenon as well. Overall, this hypothesis is in line with the pathogenic patterns of some of the paradigmal autoimmune diseases of the nervous system, such as Sydenham's chorea and Guillain-Barré syndrome (30, 31).

At this point, there is no established animal model of NMO. Our immunization experiments using AqpZ captured several important features of the disease pathogenesis, including induction of a self-reactive anti-Aqp4 T cell response, generation of Th17 cells, and occurrence of spinal cord inflammation in areas positive for Aqp4 expression (2, 48). In addition, Abs raised against the homologous regions of AqpZ can cause astrocyte cell death in vitro and CNS inflammation upon intracranial administration. These results are in agreement with the reports indicating that Aqp4-specific T cells play an important role in the pathogenesis of NMO (51). Furthermore, some of the disease-related T cell epitopes ($Aqp4_{211–230}$) overlap with the homologous areas described by us (41). Other investigators also showed that immunization of experimental animals with $Aqp4_{207–232}$ (this is the region with most extensive homology with AqpZ) can generate self-reactive T cells capable of inducing CNS inflammation upon adoptive transfer (39). Our experiments with anti-AqpZ Abs are also consistent with past studies reporting on the biological effects of NMO IgG, including binding to the third extracellular loop of Aqp4, astrocyte cytotoxicity, complement activation, and induction of CNS inflammation (2, 13, 17–19, 42). Overall, it appears that AqpZ has encephalitogenic properties that can be important in animal modeling of NMO. Using AqpZ and Aqp4 proteins may be particularly valuable in studying the processes of cross-immunoreactivity, epitope spreading, evasion of immune tolerance, and infection-induced autoimmunity. They can also be used for induction of combined autoimmune responses in animals involving T and B cells. Such an approach may overcome some of the experimental limitations observed by us and other investigators (e.g., anti-Aqp4 Ab is not able to cross the blood–brain barrier and cause CNS inflammation in the absence of encephalitogenic T cells, and induction of T cell-mediated inflammation of the CNS alone does not cause a paralytic disease) (39). Therefore, induction of multiple effector mechanisms may better model the disease processes of NMO.

In conclusion, our study demonstrates the existence of structural homology and cross-immunoreactivity between bacterial AqpZ and human Aqp4 proteins. It also suggests that the autoimmune response against Aqp4 in NMO may be triggered by a bacterial pathogen through a mechanism of infection-induced cross-reactivity.

Supplementary Material

Refer to Web version on PubMed Central for supplementary material.

Acknowledgments

This work was supported in part by the National Institutes of Health (Grant NIH K08 NS5040901), the National Multiple Sclerosis Society (Grant RG4466-A-3 to R. Balabanov), the Hawken Family Research Fund, and the Rayman Foundation (to D.S.).

Abbreviations used in this article

Aqp	aquaporin
Cy	cyanin
DAB	diaminobenzidine
GFAP	glial fibrillary acidic protein
IP	immunoprecipitation
IPTG	isopropyl β-D thiogalactopyranoside
NMO	neuromyelitis optica
PI	postimmunization

References

1. Wingerchuk DM, Lennon VA, Lucchinetti CF, Pittock SJ, Weinshenker BG. The spectrum of neuromyelitis optica. Lancet Neurol. 2007; 6:805–815. [PubMed: 17706564]
2. Lucchinetti CF, Mandler RN, McGavern D, Bruck W, Gleich G, Ransohoff RM, Trebst C, Weinshenker B, Wingerchuk D, Parisi JE, Lassmann H. A role for humoral mechanisms in the pathogenesis of Devic's neuromyelitis optica. Brain. 2002; 125:1450–1461. [PubMed: 12076996]
3. Lennon VA, Wingerchuk DM, Kryzer TJ, Pittock SJ, Lucchinetti CF, Fujihara K, Nakashima I, Weinshenker BG. A serum autoantibody marker of neuromyelitis optica: distinction from multiple sclerosis. Lancet. 2004; 364:2106–2112. [PubMed: 15589308]
4. Pittock SJ, Lennon VA, de Seze J, Vermersch P, Homburger HA, Wingerchuk DM, Lucchinetti CF, Zéphir H, Moder K, Weinshenker BG. Neuromyelitis optica and non organ-specific auto-immunity. Arch. Neurol. 2008; 65:78–83. [PubMed: 18195142]
5. Javed A, Balabanov R, Arnason BG, Kelly TJ, Sweiss NJ, Pytel P, Walsh R, Blair EA, Stemer A, Lazzaro M, Reder AT. Minor salivary gland inflammation in Devic's disease and longitudinally extensive myelitis. Mult. Scler. 2008; 14:809–814. [PubMed: 18573828]
6. Sellner J, Hemmer B, Mühlau M. The clinical spectrum and immunobiology of parainfectious neuromyelitis optica (Devic) syndromes. J. Autoimmun. 2010; 34:371–379. [PubMed: 19853412]
7. Agre P. The aquaporin water channels. Proc. Am. Thorac. Soc. 2006; 3:5–13. [PubMed: 16493146]
8. Fu D, Lu M. The structural basis of water permeation and proton exclusion in aquaporins. Mol. Membr. Biol. 2007; 24:366–374. [PubMed: 17710641]
9. Verkman AS. Aquaporins: translating bench research to human disease. J. Exp. Biol. 2009; 212:1707–1715. [PubMed: 19448080]
10. Lennon VA, Kryzer TJ, Pittock SJ, Verkman AS, Hinson SR. IgG marker of optic-spinal multiple sclerosis binds to the aquaporin-4 water channel. J. Exp. Med. 2005; 202:473–477. [PubMed: 16087714]
11. Hinson SR, Pittock SJ, Lucchinetti CF, Roemer SF, Fryer JP, Kryzer TJ, Lennon VA. Pathogenic potential of IgG binding to water channel extracellular domain in neuromyelitis optica. Neurology. 2007; 69:2221–2231. [PubMed: 17928579]
12. Bennett JL, Lam C, Kalluri SR, Saikali P, Bautista K, Dupree C, Glogowska M, Case D, Antel JP, Owens GP, et al. Intrathecal pathogenic anti-aquaporin-4 antibodies in early neuromyelitis optica. Ann. Neurol. 2009; 66:617–629. [PubMed: 19938104]
13. Cayrol R, Saikali P, Vincent T. Effector functions of antiaquaporin-4 autoantibodies in neuromyelitis optica. Ann. N. Y. Acad. Sci. 2009; 1173:478–486. [PubMed: 19758189]

14. Roemer SF, Parisi JE, Lennon VA, Benarroch EE, Lassmann H, Bruck W, Mandler RN, Weinshenker BG, Pittock SJ, Wingerchuk DM, Lucchinetti CF. Pattern-specific loss of aquaporin-4 immunoreactivity distinguishes neuromyelitis optica from multiple sclerosis. Brain. 2007; 130:1194–1205. [PubMed: 17282996]
15. Misu T, Fujihara K, Kakita A, Konno H, Nakamura M, Watanabe S, Takahashi T, Nakashima I, Takahashi H, Itoyama Y. Loss of aquaporin 4 in lesions of neuromyelitis optica: distinction from multiple sclerosis. Brain. 2007; 130:1224–1234. [PubMed: 17405762]
16. Pittock SJ, Weinshenker BG, Lucchinetti CF, Wingerchuk DM, Corboy JR, Lennon VA. Neuromyelitis optica brain lesions localized at sites of high aquaporin 4 expression. Arch. Neurol. 2006; 63:964–968. [PubMed: 16831965]
17. Sabater L, Giralt A, Boronat A, Hankiewicz K, Blanco Y, Llufriu S, Alberch J, Graus F, Saiz A. Cytotoxic effect of neuromyelitis optica antibody (NMO-IgG) to astrocytes: an in vitro study. J. Neuroimmunol. 2009; 215:31–35. [PubMed: 19695715]
18. Tani T, Sakimura K, Tsujita M, Nakada T, Tanaka M, Nishizawa M, Tanaka K. Identification of binding sites for anti-aquaporin 4 antibodies in patients with neuromyelitis optica. J. Neuroimmunol. 2009; 211:110–113. [PubMed: 19410301]
19. Iorio R, Fryer JP, Hinson SR, Fallier-Becker P, Wolburg H, Pittock SJ, Lennon VA. Astrocytic autoantibody of neuromyelitis optica (NMO-IgG) binds to aquaporin-4 extracellular loops, monomers, tetramers and high order arrays. J. Autoimmun. 2012 DOI: 10.1016/j.jaut.2012.07.008.
20. Tait MJ, Saadoun S, Bell BA, Papadopoulos MC. Water movements in the brain: role of aquaporins. Trends Neurosci. 2008; 31:37–43. [PubMed: 18054802]
21. Li L, Zhang H, Verkman AS. Greatly attenuated experimental autoimmune encephalomyelitis in aquaporin-4 knockout mice. BMC Neurosci. 2009; 10:94–99. [PubMed: 19660138]
22. Hinson SR, Roemer SF, Lucchinetti CF, Fryer JP, Kryzer TJ, Chamberlain JL, Howe CL, Pittock SJ, Lennon VA. Aquaporin-4-binding autoantibodies in patients with neuromyelitis optica impair glutamate transport by down-regulating EAAT2. J. Exp. Med. 2008; 205:2473–2481. [PubMed: 18838545]
23. Vincent T, Saikali P, Cayrol R, Roth AD, Bar-Or A, Prat A, Antel JP. Functional consequences of neuromyelitis optica-IgG astrocyte interactions on blood-brain barrier permeability and granulocyte recruitment. J. Immunol. 2008; 181:5730–5737. [PubMed: 18832732]
24. Borgnia MJ, Kozono D, Calamita G, Maloney PC, Agre P. Functional reconstitution and characterization of AqpZ, the *E. coli* water channel protein. J. Mol. Biol. 1999; 291:1169–1179. [PubMed: 10518952]
25. Calamita G, Bishai WR, Preston GM, Guggino WB, Agre P. Molecular cloning and characterization of AqpZ, a water channel from *Escherichia coli*. J. Biol. Chem. 1995; 270:29063–29066. [PubMed: 7493926]
26. Mallo RC, Ashby MT. AqpZ-mediated water permeability in *Escherichia coli* measured by stopped-flow spectroscopy. J. Bacteriol. 2006; 188:820–822. [PubMed: 16385074]
27. Fujinami RS, Oldstone MBA. Amino acid homology between the encephalitogenic site of myelin basic protein and virus: mechanism for autoimmunity. Science. 1985; 230:1043–1045. [PubMed: 2414848]
28. Kohm AP, Fuller KG, Miller SD. Mimicking the way to autoimmunity: an evolving theory of sequence and structural homology. Trends Microbiol. 2003; 11:101–105. [PubMed: 12648936]
29. Salvetti M, Giovannoni G, Aloisi F. Epstein-Barr virus and multiple sclerosis. Curr. Opin. Neurol. 2009; 22:201–206. [PubMed: 19359987]
30. Kirvan CA, Swedo SE, Kurahara D, Cunningham MW. Streptococcal mimicry and antibody-mediated cell signaling in the pathogenesis of Sydenham's chorea. Autoimmunity. 2006; 39:21–29. [PubMed: 16455579]
31. Ogawara K, Kuwabara S, Mori M, Hattori T, Koga M, Yuki N. Axonal Guillain-Barré syndrome: relation to anti-ganglioside antibodies and *Campylobacter jejuni* infection in Japan. Ann. Neurol. 2000; 48:624–631. [PubMed: 11026446]
32. Wingerchuk DM, Lennon VA, Pittock SJ, Lucchinetti CF, Weinshenker BG. Revised diagnostic criteria for neuromyelitis optica. Neurology. 2006; 66:1485–1489. [PubMed: 16717206]

33. Balabanov R, Strand K, Goswami R, McMahon E, Begolka W, Miller SD, Popko B. Interferon-gamma-oligodendrocyte interactions in the regulation of experimental autoimmune encephalomyelitis. J. Neurosci. 2007; 27:2013–2024. [PubMed: 17314297]
34. Koo HC, Park YH, Ahn J, Waters WR, Hamilton MJ, Barrington G, Mosaad AA, Palmer MV, Shin S, Davis WC. New latex bead agglutination assay for differential diagnosis of cattle infected with *Mycobacterium bovis* and *Mycobacterium avium* subsp. paratuberculosis. Clin. Diagn. Lab. Immunol. 2004; 11:1070–1074. [PubMed: 15539508]
35. Wang Y, Ren Z, Tao D, Tilwalli S, Goswami R, Balabanov R. STAT1/IRF-1 signaling pathway mediates the injurious effect of interferon-gamma on oligodendrocyte progenitor cells. Glia. 2010; 58:195–208. [PubMed: 19606498]
36. Ren Z, Wang Y, Liebenson D, Liggett T, Goswami R, Stefoski D, Balabanov R. IRF-1 signaling in central nervous system glial cells regulates inflammatory demyelination. J. Neuroimmunol. 2011; 233:147–159. [PubMed: 21257209]
37. Yong VW, Moumdjian R, Yong FP, Ruijs TC, Freedman MS, Cashman N, Antel JP. Gamma-interferon promotes proliferation of adult human astrocytes in vitro and reactive gliosis in the adult mouse brain in vivo. Proc. Natl. Acad. Sci. USA. 1991; 88:7016–7020. [PubMed: 1908086]
38. Ren Z, Wang Y, Tao D, Liebenson D, Liggett T, Goswami R, Clarke R, Stefoski D, Balabanov R. Overexpression of the dominant-negative form of interferon regulatory factor 1 in oligodendrocytes protects against experimental autoimmune encephalomyelitis. J. Neurosci. 2011; 31:8329–8341. [PubMed: 21653838]
39. Pohl M, Fischer MT, Mader S, Schanda K, Kitic M, Sharma R, Wimmer I, Misu T, Fujihara K, Reindl M, et al. Pathogenic T cell responses against aquaporin 4. Acta Neuropathol. 2011; 122:21–34. [PubMed: 21468722]
40. Nelson PA, Khodadoust M, Prodhomme T, Spencer C, Patarroyo JC, Varrin-Doyer M, Ho JD, Stroud RM, Zamvil SS. Immunodominant T cell determinants of aquaporin-4, the autoantigen associated with neuromyelitis optica. PLoS ONE. 2010; 5:e15050. [PubMed: 21151500]
41. Matsuya N, Komori M, Nomura K, Nakane S, Fukudome T, Goto H, Shiraishi H, Wandinger KP, Matsuo H, Kondo T. Increased T-cell immunity against aquaporin-4 and proteolipid protein in neuromyelitis optica. Int. Immunol. 2011; 23:565–573. [PubMed: 21795759]
42. Saadoun S, Waters P, Bell A, Vincent A, Verkman A, Papadopoulos M. Intra-cerebral injection of neuromyelitis optica immunoglobulin G and human complement produces neuromyelitis optica lesions in mice. Brain. 2010; 133:349–361. [PubMed: 20047900]
43. Feng YQ, Guo N, Huang F, Chen X, Sun QS, Liu JX. Anti-tuberculosis treatment for Devic's neuromyelitis optica. J. Clin. Neurosci. 2010; 17:1372–1377. [PubMed: 20692169]
44. Li W, Minohara M, Piao H, Matsushita T, Masaki K, Matsuoka T, Isobe N, Su JJ, Ohyagi Y, Kira J. Association of anti-*Helicobacter pylori* neutrophil-activating protein antibody response with anti-aquaporin-4 autoimmunity in Japanese patients with multiple sclerosis and neuromyelitis optica. Mult. Scler. 2009; 15:1411–1421. [PubMed: 19965522]
45. Papais-Alvarenga RM, Miranda-Santos CM, Puccioni-Sohler M, de Almeida AM, Oliveira S, Basilio De Oliveira CA, Alvarenga H, Poser CM. Optic neuromyelitis syndrome in Brazilian patients. J. Neurol. Neurosurg. Psychiatry. 2002; 73:429–435. [PubMed: 12235313]
46. van de Veerdonk FL, Gresnigt MS, Kullberg BJ, van der Meer JW, Joosten LA, Netea MG. Th17 responses and host defense against microorganisms: an overview. BMB Rep. 2009; 42:776–787. [PubMed: 20044948]
47. Axtell RC, Raman C, Steinman L. Interferon-β exacerbates Th17-mediated inflammatory disease. Trends Immunol. 2011; 32:272–277. [PubMed: 21530402]
48. Li Y, Wang H, Long Y, Lu Z, Hu X. Increased memory Th17 cells in patients with neuromyelitis optica and multiple sclerosis. J. Neuroimmunol. 2011; 234:155–160. [PubMed: 21489641]
49. Varrin-Doyer M, Spencer CM, Schulze-Topphoff U, Nelson PA, Stroud RM, Cree BAC, Zamvil SS. Aquaporin 4-specific T cells in neuromyelitis optica exhibit a Th17 bias and recognize *Clostridium* ABC transporter. Ann. Neurol. 2012; 72:53–64. [PubMed: 22807325]
50. Zéphir H, Fajardy I, Outteryck O, Blanc F, Roger N, Fleury M, Rudolf G, Marignier R, Vukusic S, Confavreux C, et al. Is neuromyelitis optica associated with human leukocyte antigen? Mult. Scler. 2009; 15:571–579. [PubMed: 19299434]

51. Warabi Y, Yagi K, Hayashi H, Matsumoto Y. Characterization of the T cell receptor repertoire in the Japanese neuromyelitis optica: T cell activity is up-regulated compared to multiple sclerosis. J. Neurol. Sci. 2006; 249:145–152. [PubMed: 16860825]

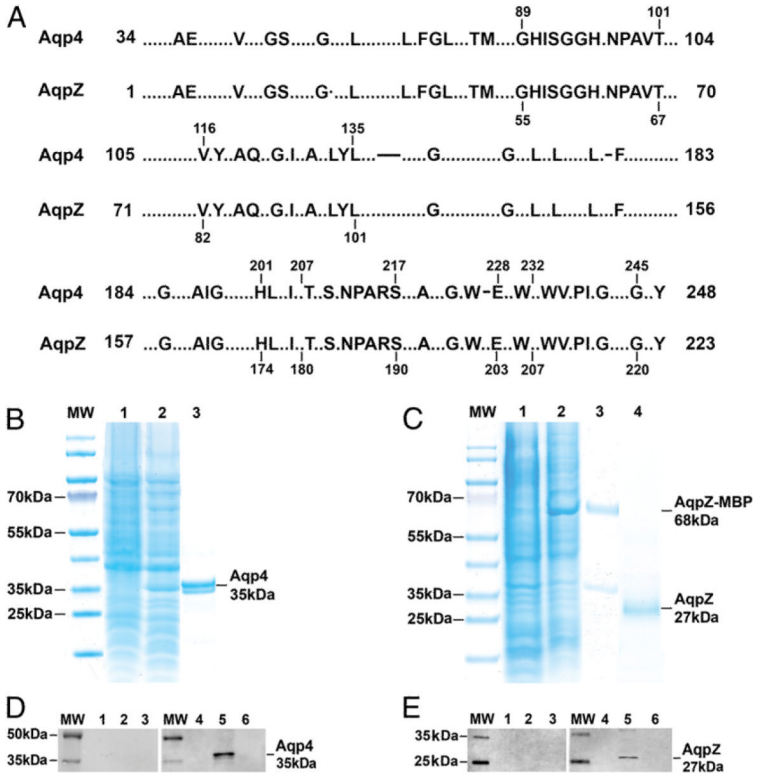

FIGURE 1.

Structural homology between Aqp4 and AqpZ proteins. (**A**) Sequence alignment of Aqp4 and AqpZ proteins. Letters indicate the homologous residues, and dots represent the nonhomologous residues. Short lines mark alignment interruptions. (**B**) Purification of Aqp4 protein: 1, a lysate from an uninduced bacterial culture; 2, a lysate from an IPTG-induced bacterial culture; 3, a purified Aqp4 protein. (**C**) Purification of AqpZ protein: 1, a lysate from an uninduced bacterial culture; 2, a lysate from an IPTG-induced bacterial culture; 3, a purified AqpZ–MBP fusion protein; 4, a purified AqpZ protein. (**D**) Western blot of Aqp4 with an isotype IgG control (*lanes 1–3*) and a commercial anti-Aqp4 Ab (*lanes 4–6*). *Lanes 1* and *4*, No sample; *lanes 2* and *5*, Aqp4 protein; *lanes 3* and *6*, an irrelevant protein (trypsin inhibitor). (**E**) Western blot of AqpZ with control (*lanes 1–3*) and immune (AqpZ) mouse (*lanes 4–6*) sera; *lanes 1* and *4*, no sample; *lanes 2* and *5*, AqpZ protein; *lanes 3* and *6*, trypsin inhibitor; 8–16% SDS-PAGE. MW, Molecular weight markers.

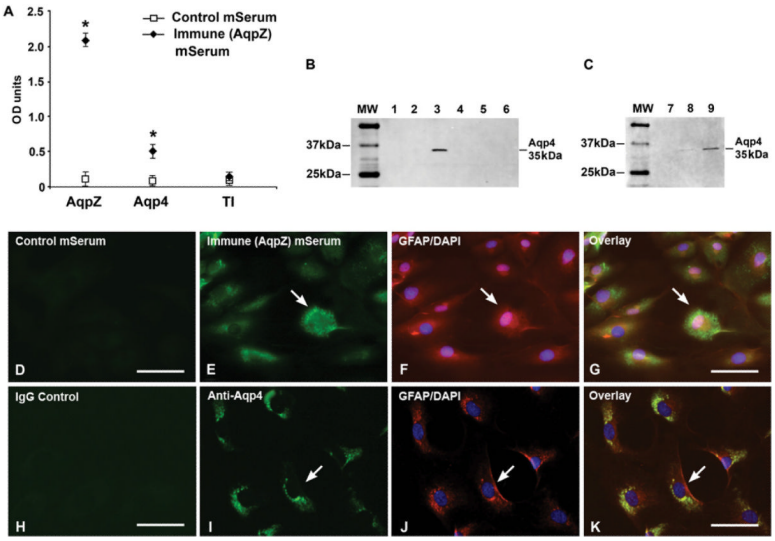

FIGURE 2.

Cross-reactivity of immune (AqpZ) mouse serum with Aqp4 protein. (**A**) Indirect ELISA with AqpZ, Aqp4, and an irrelevant protein (trypsin inhibitor [TI]), as well as immune (AqpZ) or control mouse sera; 1:100 serum dilution, 10 μg/well protein concentration ($n = 3$ measurements). (**B** and **C**)IP of Aqp4 with mouse (*lanes 1–6*) and human (*lanes 7–9*) sera (1:10 dilution). *Lane 1*, No sample; *lane 2*, IP of Aqp4 from IPTG-induced bacterial cultures with control mouse serum; *lane 3*, IP of Aqp4 from IPTG-induced bacterial cultures with immune mouse serum; *lane 4*, a cell lysate from uninduced bacterial cultures; *lane 5*, IP of trypsin inhibitor with control mouse serum; *lane 6*, IP of trypsin inhibitor with immune (AqpZ) mouse serum; *lane 7*, no sample; *lane 8*, IP of Aqp4 from IPTG-induced bacterial cultures with control human serum; *lane 9*, IP of Aqp4 from IPTG-induced bacterial cultures with NMO serum. Aqp4 detection was performed using a commercial anti-Aqp4 Ab; 8–16% SDS-PAGE. Immunostaining of human astrocytes cultures (nonpermeabilized) with control mouse serum (1:100 dilution) (**D**) and a control (isotype) IgG (**H**). Dual immunostaining of the cultures with immune (AqpZ) mouse serum (**E**–**G**) or a commercial anti-Aqp4 Ab (**I**–**K**) (FITC, green), concurrently with an anti-GFAP Ab (Cy3, red) and DAPI nuclear stain (blue). Arrows point to cells with signal colocalization. Scale bars, 40 μm. *$p < 0.05$. MW, Molecular weight markers.

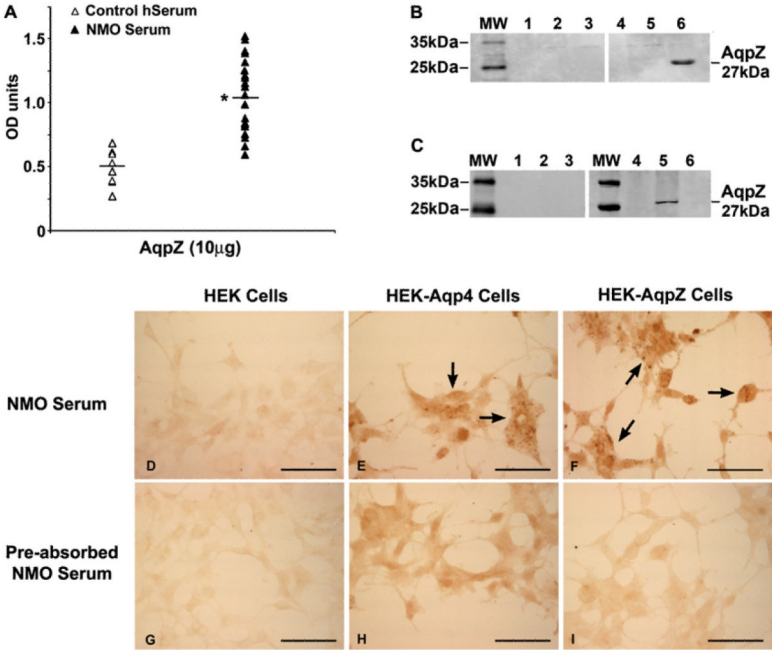

FIGURE 3.

Cross-reactivity of NMO sera with AqpZ protein. (**A**) Indirect ELISA with AqpZ (10 μg) and NMO (*n* = 20 samples) or control human (*n* = 9 samples) sera (1:100 dilution). (**B**) Western blot of AqpZ with control human (*lanes 1–3*)and NMO (*lanes 4–6*) sera. *Lanes 1* and *4*, No sample; *lanes 2* and *5*, an irrelevant protein (trypsin inhibitor); *lanes 3* and *6*, AqpZ protein. (**C**) Western blot of AqpZ with an isotype IgG (*lanes 1–3*) and a commercial anti-Aqp4 Ab (*lanes 4–6*). *Lanes 1* and *4*, No sample; *lanes 2* and *5*, AqpZ protein; *lanes 3* and *6*, trypsin inhibitor; 8–16% SDS-PAGE, Indirect immunostaining (brown, DAB) of HEK cells (**D**, **G**) and HEK cells (nonpermeabilized) overexpressing Aqp4 (**E**, **H**) and AqpZ (**F**, **I**) with NMO serum (1:100 dilution) before (D–F) and after preabsorption (G–I) with AqpZ protein. Arrows point to positive cells. Scale bars, 50 μm. *p < 0.05. MW, Molecular weight marker.

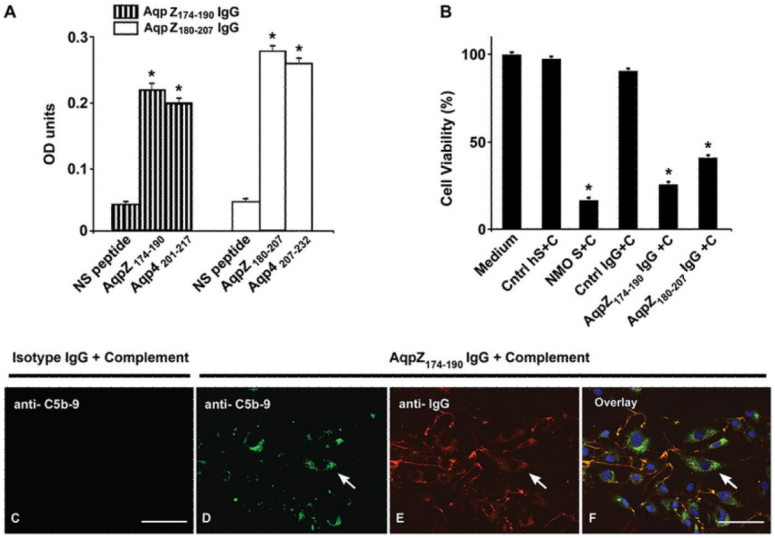

FIGURE 4.

Cross-reactivity and cytotoxicity of anti-AqpZ IgGs. (**A**) Indirect ELISA with anti-$AqpZ_{174–190}$ and anti-$AqpZ_{180–207}$ IgGs (1:5000 dilution) and the corresponding $AqpZ_{174–190}$, $AqpZ_{180–207}$, or homologous $Aqp4_{201–217}$ and $Aqp4_{207–232}$ peptides (2 μg); nonhomologous $AqpZ_{67–80}$ peptide was used as anonspecific (NS) control. (**B**) Cell-viability (MTT) assay of human astrocyte cultures (1×10^5 cells/well) treated with medium only, control human or NMO sera (S) (1:3 dilution), a control (isotype) IgG, or anti-$AqpZ_{174–190}$ or anti-$AqpZ_{180–207}$ IgG (50 μg/ml) in the presence of complement (+C) (1:50 dilution) (n = 3 measurements). Dual immunostaining of human astrocyte cultures that were treated with an isotype IgG control (**C**) or an anti-$AqpZ_{174–190}$ IgG (**D**–**F**) and complement, with anti–C5b-9 (FITC, green, C, D) and anti-IgG (Cy3, red, E) Abs and DAPI nuclear staining (blue). Arrows point to signal colocalization. Scale bars, 40 μm. *$p < 0.05$.

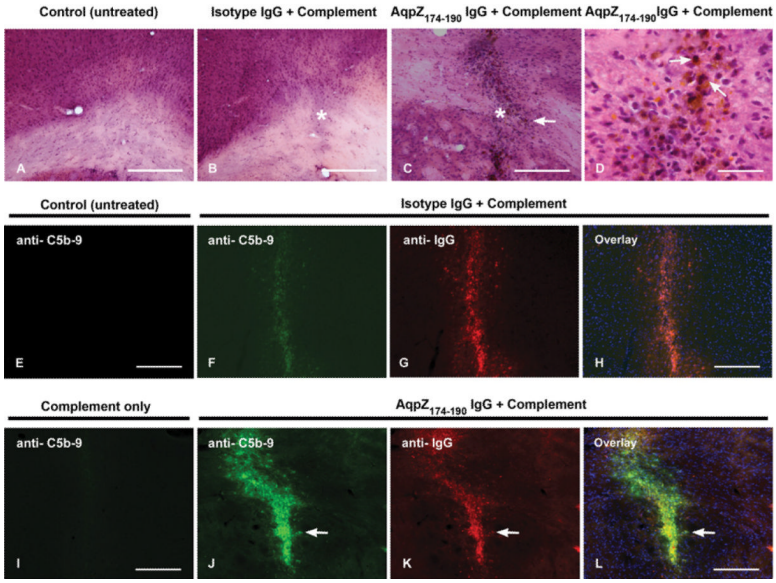

FIGURE 5.

Induction of CNS inflammation by $AqpZ_{174–190}$ IgG. H&E staining of brain tissue of an untreated (control) mouse (**A**) and mice injected with either an isotype IgG control (**B**) or an $AqpZ_{174–190}$ IgG (**C**, **D**) (8 μg) and complement (2 μl). Asterisks mark the injection sites, and the arrows point to the inflammatory cells. Scale bars in (A)–(C), 200 μm; scale bar in (D), 50 μm. Dual immunostaining of brain tissue of an untreated (control) mouse (**E**) and mice injected with an isotype IgG and complement (**F**–**H**), complement only (**I**), or an $AqpZ_{174–190}$ IgG and complement (**J**–**L**). Anti–C5b-9(FITC, green) (E, F, I, J) and anti-IgG (Cy3, red) (G, K) Abs and DAPI nuclear staining (blue). Arrows point to signal colocalization. Scale bars, 150 μm.

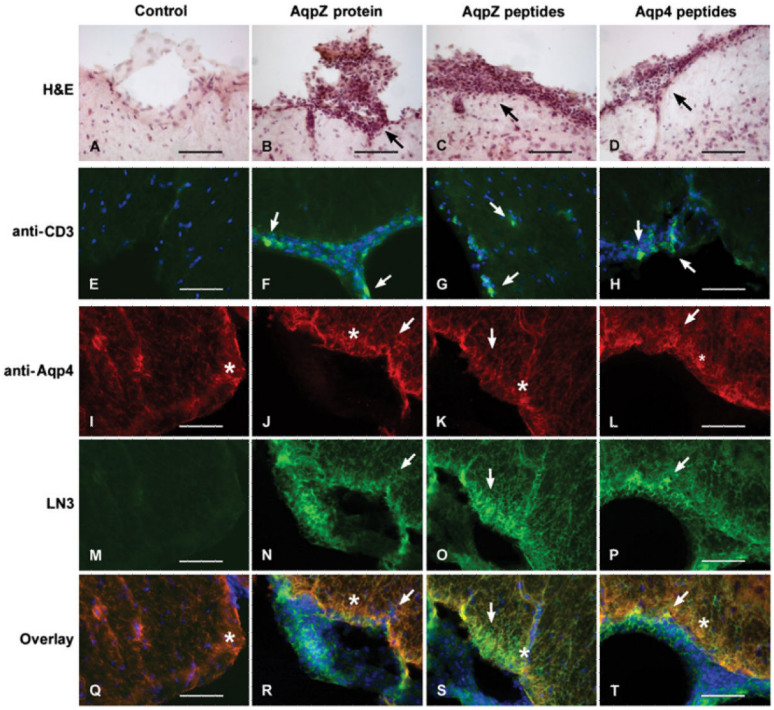

FIGURE 6.

Mouse immunization with AqpZ-induced CNS inflammation. H&E staining of spinal cords of a control (CFA-injected) mouse (**A**) and mice immunized with AqpZ protein (**B**), a mixture of homologous AqpZ (**C**), and homologous Aqp4 (**D**) peptides. Arrows point to areas of inflammation. Scale bars, 150 μm. Immunostaining of spinal cords of a control (CFA-injected) mouse (**E**) and mice immunized with AqpZ protein (**F**), a mixture of homologous AqpZ (**G**), and homologous Aqp4 (**H**) peptides with an anti-CD3 (FITC, green, E–H) Ab and DAPI nuclear staining (blue). Arrows point to $CD3^+$ cells. Scale bars, 50 μm. Dual immunostaining of the same control (**I**, **M**, **Q**) and immunized mice, AqpZ protein (**J**, **N**, **R**), homologous AqpZ (**K**, **O**, **S**), and homologous Aqp4 (**L**, **P**, **T**) peptides with anti-Aqp4 (Cy3, red, I–L) and LN3 (FITC, green, M–P) Abs and DAPI nuclear staining (blue). Asterisks mark the areas of Aqp4 positivity, and the arrows point to the $LN3^+$ cells. Scale bars, 50 μm.

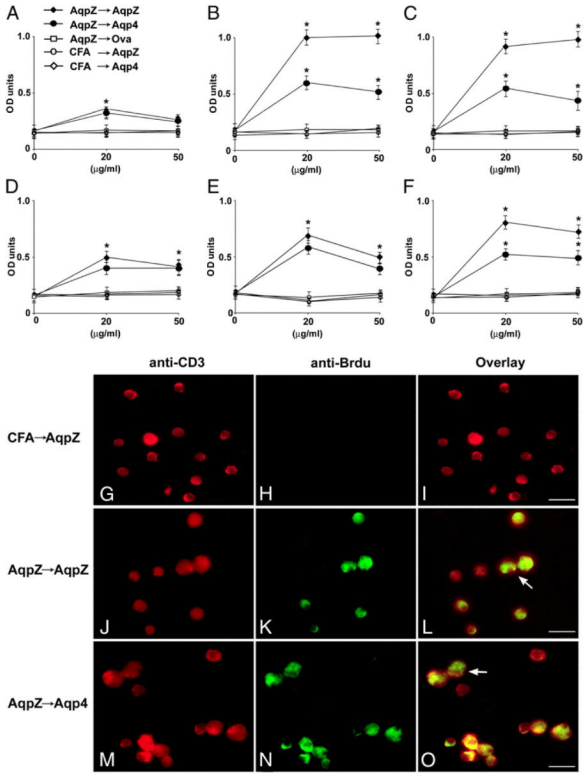

FIGURE 7.

Lymphocyte-proliferation assay. Lymphocyte-proliferation assay was performed at day 8 PI using purified spleen T cells from mice immunized separately with $AqpZ_{82–101}$ (**A**), $AqpZ_{174–190}$ (**B**), and $AqpZ_{203–220}$ (**C**) peptides that were stimulated in vitro with the corresponding priming AqpZ (Aqp-Z→AqpZ), a nonpriming but homologous Aqp4 (AqpZ→Aqp4), or a nonpriming and nonhomologous $OVA_{323–339}$ (AqpZ→OVA) peptide (0–50 μg/ml/72 h). T cells from CFA-injected mice were similarly stimulated with all four pairs of homologous AqpZ (CFA→AqpZ) and Aqp4 (CFA→Aqp4) peptides. (**D**–**F**) Lymphocyte-proliferation assay was similarly performed using T cells from mice immunized with AqpZ protein. They were stimulated as above with $AqpZ_{82–101}$ (D), $AqpZ_{174–190}$ (E), and $AqpZ_{203–220}$ (F) peptides; their corresponding homologous Aqp4 peptides; and nonhomologous $OVA_{323–339}$. T cells derived from CFA-injected mice were stimulated with each pair of homologous peptides ($n = 3$ animals/group). (**G**–**O**) Immunostaining of cell samples from the $AqpZ_{174–190}$ lymphocyte-proliferation assay [corresponding to (B)] with anti-CD3 (Cy3, red) and anti-BrdU (FITC, green) Abs. Arrows point to proliferating $CD3^+/BrdU^+$ cells. Scale bars, 50 μm. *$p < 0.05$.

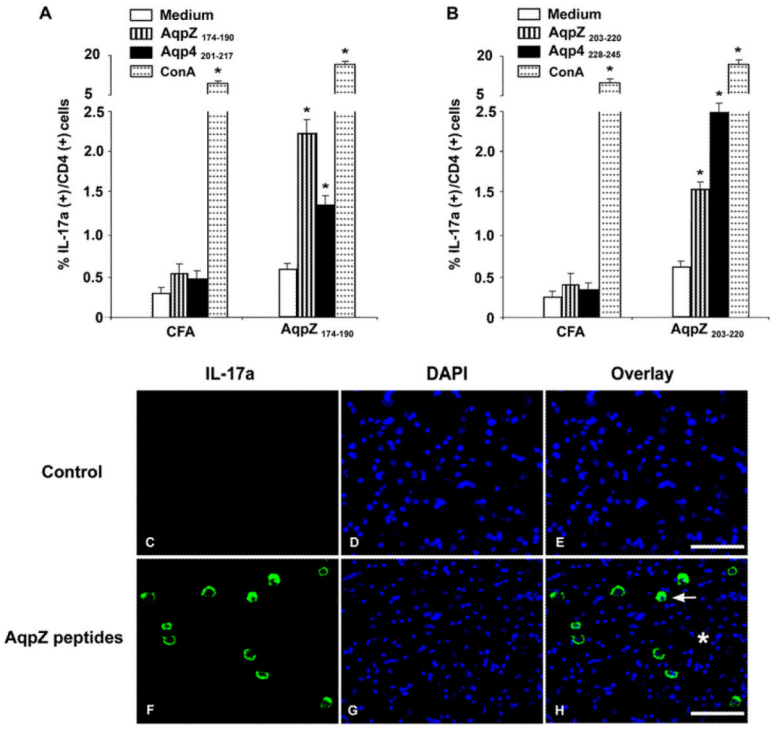

FIGURE 8.

Changes in the IL-17a$^+$/CD4$^+$ cell populations in response to AqpZ peptides. T cells from mice immunized with AqpZ$_{174–190}$ (**A**) and AqpZ$_{203–220}$ (**B**) peptides and CFA-injected mice were stimulated in vitro with medium only, the priming AqpZ and the corresponding homologous Aqp4 peptides (20 μg/ml), and Con A (5 μg/ml) for 72 h. The percentage of IL-17a$^+$/CD4$^+$ cells was measured using flow cytometry (n = 3 animals/group). Immunostaining of spinal cords of a control (CFA-injected) mouse (**C**–**E**) and a diseased mouse immunized with homologous AqpZ peptides (**F**–**H**), with an anti–IL-17a (FITC, green) Ab and DAPI nuclear staining (blue). Arrow points to IL-17a$^+$ cells; the asterisk marks the blood vessel. Scale bars, 100 μm. *$p < 0.05$.